Volume xx (200y), Number z, pp. 1–12

Visual Quantification of the Circle of Willis: An Automated Identification and Standardized Representation

H. Miao[1], G. Mistelbauer [1], C. Našel[2] and M. E. Gröller[1,3]

[1]Technische Universität Wien, Austria
[2]Karl Landsteiner University of Health Sciences, Austria
[3]VRVis Research Center, Austria

Abstract

This paper presents a method for the visual quantification of cerebral arteries, known as the Circle of Willis (CoW). It is an arterial structure with the responsibility of supplying the brain with blood, however, dysfunctions can lead to strokes. The diagnosis of such a time-critical/urgent event depends on the expertise of radiologists and the applied software tools. They use basic display methods of the volumetric data without any support of advanced image processing and visualization techniques. The goal of this paper is to present an automated method for the standardized description of cerebral arteries in stroke patients in order to provide an overview of the CoW's configuration. This novel representation provides visual indications of problematic areas as well as straightforward comparisons between multiple patients. Additionally, we offer a pipeline for extracting the CoW from Time-of-Flight Magnetic Resonance Angiography (TOF-MRA) data sets together with an enumeration technique for labeling the arterial segments by detecting the main supplying arteries of the CoW. We evaluated the feasibility of our visual quantification approach in a study of 63 TOF-MRA data sets and compared our findings to those of three radiologists. The obtained results demonstrate that our proposed techniques are effective in detecting the arteries and visually capturing the overall configuration of the CoW.

Categories and Subject Descriptors (according to ACM CCS): I.4.0 [Image Processing and Computer Vision]: General—Image processing software; J.3 [Computer Applications]: Life and Medical Sciences—Health

1. Introduction

The human brain is a very delicate structure that is highly dependent on a well-functioning blood supply. A vascular disease in the brain can lead to a stroke, which is the second most common cause of death and the major cause of acquired disability in the developed world [The16b]. Stroke treatment relies on the application of imaging techniques and the investigations done by radiologists. The focus of an examination lies hereby on the arterial blood supply, which is guaranteed by the Circle of Willis (CoW). This arterial circle is depicted in Figure 1. The radiologist inspects the TOF-MRA data set (hereby simply referred to as data set) using traditional display methods, such as slice-by-slice views and Maximum Intensity Projection (MIP) to identify the cause of a dysfunction. This diagnostic process is complicated due to its urgent nature and the time-constraints of stroke treatment. In contrast, the process is time-consuming and every patient is viewed as a case of its own without considering preexistent cases. Side-by-side comparisons are impeded by the traditional display methods. As the CoW exhibits a high variability across different patients, its shape and topology are highly relevant for stroke assessment. To support stroke assessment in a timely manner, we propose a standardized visualization of the CoW, rectifying the above shortcomings. The main contributions of our work are:

- A fully automatic CoW extraction pipeline
- A systematic description of the CoW
- A standardized visualization of the CoW
- A visual indication of problematic areas of the CoW
- An efficient comparison of multiple patients

The above mentioned features are combined in a visualization, that we call the Circle of Willis Radar/Radial Visualization (CoWRadar). It is not only targeted at the initial assessment of strokes but it could also be potentially useful at the treatment stage, where it is still often required to have an overview of the CoW.

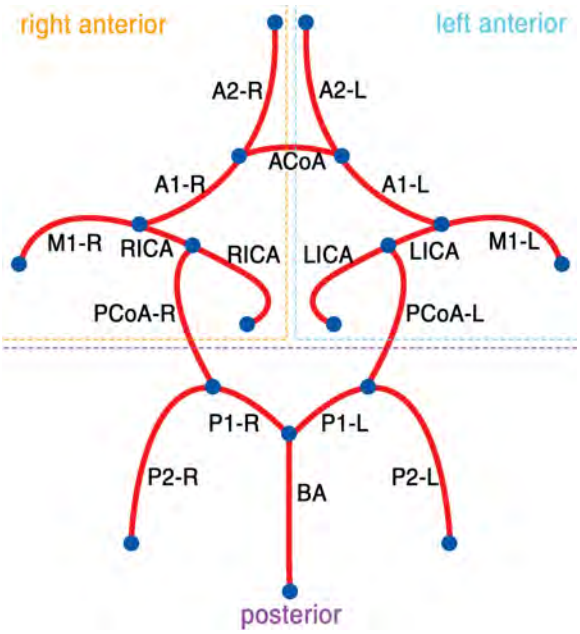

Figure 1: A schematic representation of the CoW standard configuration with anatomically-correct labeled arteries and a subdivision into three parts.

2. Related Work

In this paper we use established image processing methods but also introduce novel methods that are required for the visual quantification of the CoW. The standardized visualization of the CoW relies on a vascular model , referred to as *vessel graph*, that has to be extracted first. The most closely related methods and algorithms for the proposed pipeline, as shown in Figure 2, are described in this section. A general introduction to medical image processing and visualization is given by Preim and Botha [PB13].

Standardized representations in medical visualization have already been addressed for several anatomical structures. Termeer et al. [TBB*07] presented the volumetric bull's eye plot, where the cardiac muscle wall is unfolded to visualize scar tissue. Neugebauer et al. [NGB*09] describe a map display to interactively show scalar flow features of cerebral aneurysms by combining a 3D model of the vascular anatomy with surrounding 2D maps. Hartkamp and Van der Grond [HvdG00] investigated morphological variations of the CoW using Magnetic Resonance Angiography (MRA). The authors describe different variations of the standard configuration.

Kirbas and Quek [KQ03] reviewed vessel extraction methods targeted at neurovascular structures. They divided the algorithms into six main categories: pattern-recognition techniques, model-based approaches, tracking-based approaches, artificial intelligence-based approaches, neural network-based approaches, and miscellaneous tube-like object detection approaches. Pock describes in his master's thesis rules to convert centerlines to a graph representation [Poc04]. Motivated by this approach, we similarly convert the segmented blood vessels of the CoW into a vessel graph in order to propose a systematic description afterwards. Our segmentation is based on the Hysteresis Thresholding (HT) method by Canny [Can86], which requires two parameters: A high and a low threshold value. Both values can be estimated by a histogram analysis, as described by Condurache and Aach [CA05].

The CoW is supplied by three main arteries and can be divided into three parts, each responsible for the blood transport to a separate area of the brain. The segmentation result has to be separated into the same three parts, in order to reflect this natural division of the CoW. In the work of Bullitt et al. [BMJ*05] the authors described a method for the subdivision of the intracranial circulation into four vessel clusters. The centerline extraction or skeletonization is a first step in vessel modeling. A skeletonization approach based on topological thinning was introduced by Lee et al. [LKC94]. Vascular structures are commonly modeled as a vessel graph with edges and nodes that represent segments and branching points. A detailed vessel model is described by Mistelbauer [Mis13], which is also used in this work.

An automated labeling of the CoW is proposed by Bogunovic [Bog12]. His approach is concerned with identifying the anatomically correct names of the bifurcations by using a maximum a-posteriori estimation. He evaluated his automated approach on a set of 50 images of healthy patients and reported to have labeled 60% of the cases entirely correct. However, his technique favors sensitivity over specificity and rather tends to find a false bifurcation than to miss one, which is a potential weak point. Tang and Chung [TC06] proposed a tree-matching algorithm for 3-D rotational X-ray angiography data based on the concept of a theoretical tree edit distance. A method to create planar visualizations of blood vessels and airways is described by Marino and Kaufman [MK16].

The CoW can be described by multiple vascular trees (one tree per supplying artery) that are connected at their leaves nodes. Motivated by the circular layout of the CoW, a radial graph layout is an appropriate choice to display the branching structure and topology of the CoW comprehensibly. Draper et al. [DLR09] described radial design methods as visualizations that arrange data in an elliptical fashion and identified different design patterns. The *Handbook of Graph Drawing and Visualization* by Tamassia [Tam14] gives a survey of current graph drawing algorithms and visualizations.

This work is an extended version of the paper by the same authors [MMNG15]. The pipeline, see Figure 2, was extended to increase the comprehensibility of the processing steps. We added another use case in order to show the correspondence between the labeled vessel graph and the CoWRadar.

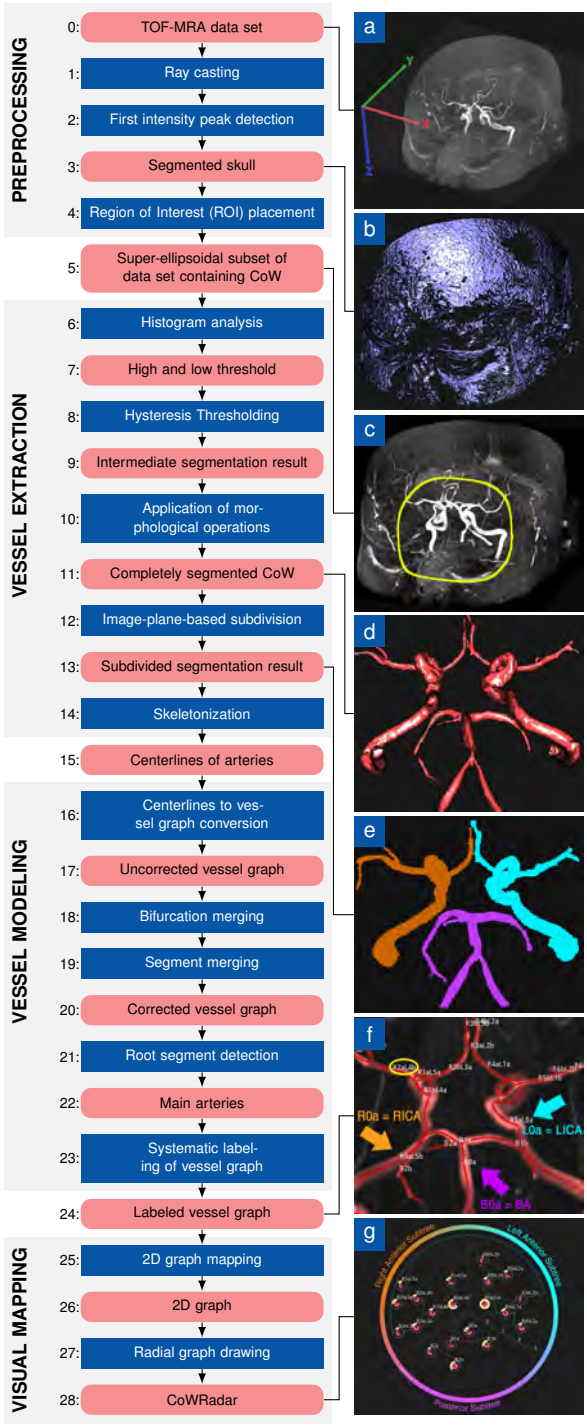

Figure 2: Our fully automatic pipeline for visual quantification of the CoW. It consists of a sequence of operations that are sequentially executed. Intermediate results are shown with the images on the right.

3. Morphology and Topology of the CoW

For stroke treatment radiologists are interested in the blood supply of the brain tissue and, consequently, in the CoW. The identification of the collateral blood flow is especially important. By inspecting medical data sets, physicians are able to locate the source of the stroke and decide upon suitable treatment strategies.

The CoW can be naturally separated into three parts that we refer to as *subtrees*. See Figure 1 for the standard configuration of the CoW. Each subtree is primarily supplied by one main artery. The Left Internal Carotid Artery (LICA) supplies the left anterior subtree, the Right Internal Carotid Artery (RICA) supplies the right anterior subtree and the Basilar Artery (BA) supplies the posterior subtree. Other important arteries are the A1 segment of the Anterior Cerebral Artery (A1), the M1 segment of the Middle Cerebral Arteries (M1) and the P1 segment of the Posterior Cerebral Artery (P1). The subtrees are connected to form a circle by the communicating arteries to create a collateral blood supply. The anterior subtrees are connected by the Anterior Communicating Artery (ACoA) and the posterior subtree is connected to the anterior subtrees by the left and right Posterior Communicating Arteries (PCoAs). The communicating arteries (ACoA and PCoAs) provide valuable information about the collateral blood circulation whereas the main arteries ensure the supply of a major part of the brain.

4. Data Acquisition

As data acquisition modality we use 3D Time-of-Flight Magnetic Resonance Angiography (TOF-MRA) (see Figure 2). It is typically applied to acquire high-resolution data sets of stroke patients without the need to administer a contrast agent to capture blood vessels. According to Hartung et al. [HGF11] the signal from stationary tissue is saturated by excitation pulses, resulting in a suppressed background signal. The incoming blood will be free of the excitation pulse and therefore have a high signal intensity. This method has a high signal-to-noise ratio, but turbulent or slow flow can cause signal loss from blood vessels. As a result, these vessels are represented by only low intensity values.

5. Methodology

We propose a visual indication of problematic areas and a simple standardized display of a patient's CoW. In order to relieve radiologists of tediously inspecting the entire data set, we propose a fully automated pipeline that processes TOF-MRA data sets to create appropriate standardized visualizations of the CoW (see Figure 2). We developed a software solution for the clinical practice that does not introduce additional working steps.

Firstly, in a preprocessing step, we identify the skull bone of the patient and derive the Region of Interest (ROI) containing the CoW. In the second step, we extract the main

arteries of the CoW. Thirdly, we convert the intensity-based representation of the blood vessels into a graph. We introduce a novel method for the systematic labeling of this vessel graph. Finally and fourth, we visually map the vessel graph to a standardized radial layout that we refer to as *CoWRadar*. Subsequently, each of these steps is explained in detail.

5.1. Preprocessing

We need to preprocess the TOF-MRA data sets in order to extract the blood vessels of the CoW. The intensity values in the provided data vary between 0 and 962. The overlapping intensity ranges of the skull and arteries lead to problems for the HT-based segmentation-approach. Hence, the skull needs to be excluded from further processing. We segment the skull by shooting rays from the outside of the data sets to the inside and look for the first intensity peak along the rays. However, the human skull has holes in the eye sockets and the base of the skull that allow rays to pass through. Therefore, rays are only shot laterally into the volume. For both lateral directions, the rays will hit the skull first before reaching the brain and its arteries. The bones are hereby detected by using a threshold of 150, which is an empirically motivated value that has been suitable for all of our results. Once all rays have been cast, the location of the skull can be estimated by considering the intensity peaks that were detected first along the rays. They give a rough estimation of the skulls's location (see Figure 2b).

Then, we place a super-ellipsoidal ROI that includes the CoW (see Figure 2c). The location and size of the ROI are based on an empirically defined ratio determined from the skull. This shift and scaling of the super-ellipsoid is defined by considering the average location and size of the CoW in the provided data (12 TOF-MRAs). The center (c_x, c_y, c_z) of the skull-voxels is computed as the mean of the skull-voxel positions. The center of the ROI (p_x, p_y, p_z) is shifted from (c_x, c_y, c_z) by using the following empirically motivated factors: $p_x = c_x \cdot 1.02$, $p_y = c_y \cdot 0.78$ and $p_z = c_z \cdot 1.2$.

This heuristic guarantees the placement of the ROI in close proximity to all arteries of the CoW. Next, the shape of the ROI has to be adjusted. The goal is to cover the entire CoW, but not too much of the surrounding tissue. This is done by setting the semi-axes A, B and C of the suggested super-ellipsoid. For this purpose, the average Euclidean distance r between (c_x, c_y, c_z) and the skull-voxel positions are computed. r is thereby regarded as an approximative radius of the skull. The semi-axes are then empirically calculated as follows: $A = r \cdot 0.52$, $B = r \cdot 0.46$ and $C = Z \cdot 0.52$, where Z defines the extent of the data set along the z-axis. Since the skull is not entirely covered by the scan, the C-parameter of the super-ellipsoid is adjusted by using Z instead of r. The detected ROI covering the CoW specifies the spatial range of our subsequent approach. By adjusting the axes-lengths, the size and the roundedness of the super-ellipsoid, differently shaped CoWs can be covered.

5.2. Vessel Extraction

The arteries are represented by voxels and their intensity values inside the ROI. In order to create a vascular model, we distinguish between artery and background voxels. We extract the vessel centerlines, which are good abstractions for the arteries due to their tubular structure.

The arteries are segmented using HT and the result is shown in Figure 2d. This work suggests a histogram-based estimation of the thresholds that is related to the work of Condurache and Aach [CA05]. Our method solely analyzes the histogram of the voxels inside the ROI for the automated estimation of the two thresholds. Empirical percentiles around 98.8% for the low threshold and 99.9% for the high threshold have shown to produce good results.

The segmentation result is then divided into three parts in order to reflect the natural subdivision of the CoW into three subtrees. We thereby project the segmentation result along the x-, y- and z-axis, reducing the data sets to three image planes, which are shown in Figure 3. We exploit the shape and arrangement of the arteries in the two-dimensional image planes.

Initially, we separate the segmentation result in each of the three planes. Then, we use the results from the three individual planes to determine the subdivision of the segmentation result in the 3D volume. In Figure 3 the orange part is associated with the right anterior subtree, the cyan part with the left anterior subtree and the violet part with the posterior subtree. The separation into subdivisions is performed in the three planes by using reference points, which are based on the shape and location of the super-ellipsoidal ROI. The pixels in the sagittal and transverse planes are assigned to the closest reference point.

In the **coronal plane** the right and left anterior reference points are at $(p_x + A, p_z)$ and $(p_x - A, p_z)$. Using the image planes, a rough estimation of the BA's location can be done. As the coronal plane in Figure 3a shows, the BA is normally located in-between the two carotid arteries. This fact is exploited to get a better approximation of the location of the BA on the x-axis. For this reason, a ray casting method is additionally applied. Rays are shot from left and right. After the first object is hit, the ray terminates if it hits a background point. Finally, the center c_{BA} of the left (cyan) and right (orange) areas are calculated as an approximation of the BA's location on the x-axis.

The **sagittal plane** is used to assign the P1 segments to the posterior subtree. The reference points are at $(p_y + B, p_z - C)$ and $(p_y - B, p_z + C)$ and the result is shown in Figure 3b.

In the **transverse plane** the posterior reference point is defined by $(c_{BA}, p_y + B)$, the left anterior reference point is located at $(c_{BA} + A, p_y - B)$, and the right anterior reference point is positioned at $(c_{BA} - A, p_y - B)$. Only those voxels that have not been marked already in the sagittal and coronal planes are considered. The result is shown in Figure 3c.

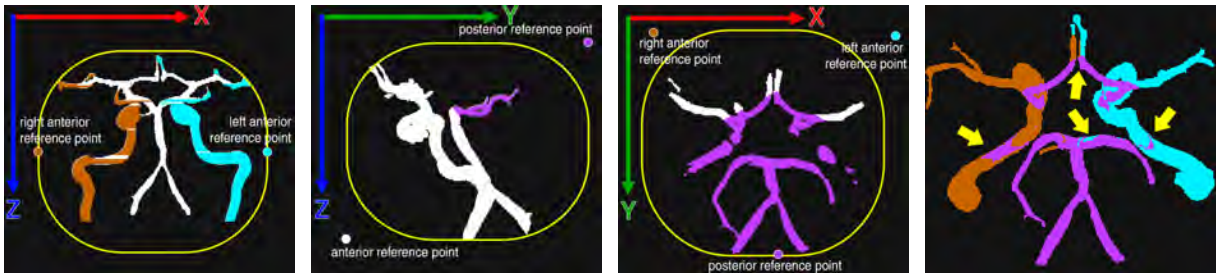

(a) Coronal plane (b) Sagittal plane (c) Transverse plane (d) Marked segmentation result

Figure 3: The three image planes of the segmentation result and the initial subdivision. (a) displays the coronal plane, where the left and right anterior parts are marked. (b) displays the sagittal plane, which is used to mark the P1 segments in the posterior subtree. (c) shows the transverse plane where the posterior part is marked. (d) shows the segmentation result marked according to the image planes. The arrows point to small areas that are not assigned to the correct subtree yet.

The subdivision of the segmentation result in the 3D volume is then determined according to the results from the image planes in the following order: transverse, coronal and sagittal. If a segmented voxel is marked twice, the last marking is taken. After this procedure, some small parts are still incorrectly assigned as shown in Figure 3d. To address this issue, we apply the following approach: We determine the largest connected components of each of the three parts and take them as the initial areas. Then, these initial areas grow in a breadth-first manner and absorb parts that do not belong to another initial area. The final result is displayed in Figure 2e, which shows the correct separation of the segmentation result into the three subtrees.

This approach allows us to quickly perceive the absence of a main artery. In such a case, a major part of the brain is potentially under-supplied with blood, which is a highly relevant information for the domain experts. The main arteries are the largest arteries of the CoW. Their presence can be detected by comparing the different (colored) parts in the image planes with each other. The transverse MIP in Figure 4a shows an example data set with a missing LICA according to the domain expert. If the left or right part in the coronal plane is relatively small, then we assume that a main artery is missing, as illustrated in Figure 4b. Compared to the example in Figure 3a, this CoW is not symmetric since the LICA is missing. The area of the cyan left anterior part is smaller than the area of the orange right anterior part. As a result, the CoW is separated into two subtrees instead of three, in order to reflect this irregular blood circulation, where the left anterior part of the brain seems to be under-supplied. (see Figure 4c). The smaller cyan area is then discarded since we assume that these smaller arteries are not supplied by the LICA.

In order to provide a sufficiently smooth segmentation for the subsequently performed skeletonization, we apply morphological operations such as closing. We use the skeletonization approach by Lee et al. [LKC94] to extract the centerlines of the arteries of the CoW.

(a) Transverse MIP (b) Coronal plane (c) Subdivided result

Figure 4: Detection of a missing main artery using the coronal plane. (a) shows the transverse MIP with an arrow pointing to the location of the missing LICA. (b) shows that the cyan area is much smaller than the orange area. (c) displays the CoW separated into two subdivisions instead of three.

5.3. Vessel Modeling

Until now, the arteries are still represented by voxel intensity values. In this section we describe methods to create a model that represents the arteries and their branching points. This model is then used as the basis for the visualization.

The centerlines are converted into a graph. The output is a representation of the CoW, which we refer to as vessel graph. The vessel graph has to be corrected in order to remove noise introduced during the segmentation and skeletonization steps. This assures a more accurate representation of the vasculature by the vessel graph.

The inaccuracies are partially due to noise in the data set and also result from the combination of the methods which we applied to extract the centerlines. We first use the skeletonization approach by Lee et al. [LKC94] for the extraction of centerlines. Then we apply the conversion rules by Pock [Poc04] to convert the centerlines to a vessel graph. In the resulting vessel graph, disconnections tend to appear. We therefore call it uncorrected vessel graph. In order to remove these errors in the topology, we propose a bifurcation

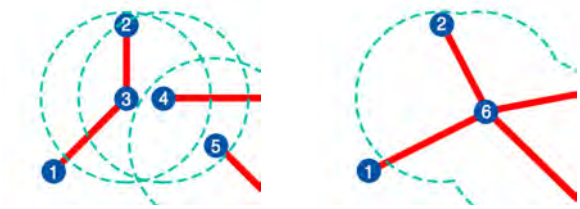

(a) Disconnected bifurcation (b) Merged bifurcation

Figure 5: Illustration of the merging of a disconnected bifurcation. The dashed circles show the search radius around the vertices 3, 4 and 5. Endpoint 2 is not merged since it is already connect to one of the initial vertices.

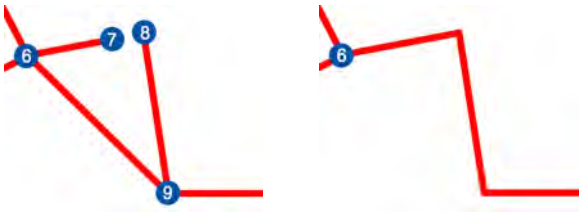

(a) Disconnected segment (b) Merged segment

Figure 6: Illustration of the segment merging and the removal of duplicate segments. Endpoints 7 and 8 are separated only by a small distance and have to be merged. After the endpoints are merged, there is a duplicated connection between vertices 6 and 9. The shorter one is removed.

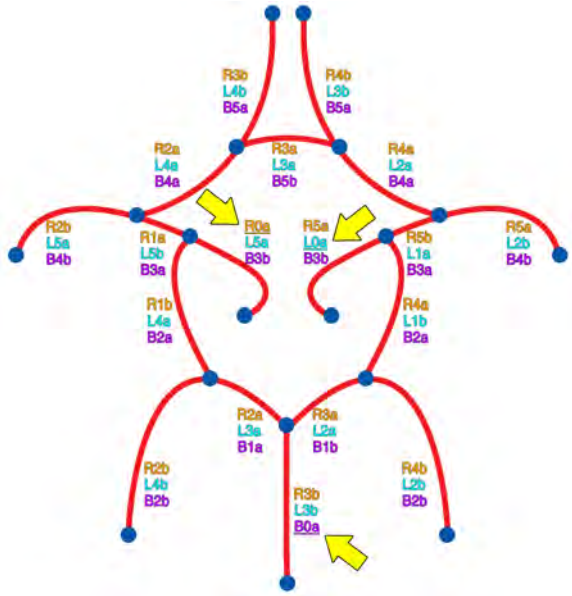

Figure 7: Systematic labeling of the standard configuration of the CoW. All segments are labeled, starting from the main arteries (root segments, shown underlined). Since the standard configuration of the CoW contains all communicating arteries, each segment receives three labeling terms. The left anterior root segment is labeled `R5a`**`L0a`**`B3b`, the right anterior root segments is labeled **`R0a`**`L5aB3b` and the posterior root segment is labeled `R3bL3b`**`B0a`**.

merging and a segment merging approach. For bifurcation merging, we connect those vertices in the uncorrected vessel graph that lie within a small distance from each other. This approach is illustrated in Figure 5.

Due to the noise in the data and errors in the segmentation, also the segments in the uncorrected vessel graph can be disconnected or falsely duplicated. For the merging of segments, a small radius around the endpoints is checked in order to look for potential endpoints to connect. If segments are merged, short duplicated connections are removed, since they are most likely noise. Figure 6 illustrates our segment merging approach. The two merging methods (Figure 5 and 6) correct the errors in the vessel graph, but in some cases they also merge bifurcations and segments where it is undesired. However, these false merges are rarely observed in the provided data sets and are, therefore, accepted for the benefit of a more accurate vessel graph.

Labeling typically refers to the assignment of the anatomically correct names to the segments of the vessel graph. We developed a different approach in collaboration with our domain expert. During the diagnosis, the radiologist is less interested in the anatomical names of the segments, but more in how the brain is supplied and, consequently, in the topology of the CoW. Neuro-radiologists can easily derive the identity of an artery by considering its connection to the supplying main artery. Based on this idea, we propose a systematic labeling of the vessel graph, starting at the main arteries, which we refer to as root segments. Each segment can be labeled based on the supplying arteries as long as there is a connection. A label consists of zero to three terms, depending on the segments connections to the main arteries. A labeling term is thereby described by the regular expression:

$$[R|L|B][0-9]^{+}[a-z] \quad (1)$$

The letters *R*, *L* and *B* specify the root segment where *R* stands for the RICA, *L* for the LICA, and *B* for the BA. The subsequent numeral specifies the number of branching points between a segment and its root segment. Lower case characters at the end indicate the branch index, which enumerates the child branches. This approach is illustrated on the standard configuration of the CoW in Figure 7. Every segment is labeled from three directions and therefore, is assigned up to three labeling terms.

Figure 2f shows a vessel graph labeled with our approach. The effectiveness of our labeling approach is illustrated on the example of the segment with the label *R2aL4b*. The *R2a* term

indicates that this particular segment is two branching points away from the RICA. The *L4b* term indicates that there is a connection between the left and right anterior subtree and the segment is four branching points away from the LICA. Therefore, it can be assumed that there is an ACoA to connect the anterior subtrees. Since the enumerator of the right labeling term is smaller than the left one, this segment is located on the right anterior subtree. Furthermore, the fact that this segment is not labeled from the BA is a clear indication that there is no connection between the anterior and posterior part. The PCoAs are absent on both sides. This relevant information can be extracted from the single segment label.

Finding the starting point of the labeling is crucial in our approach. For each subtree, the root segment must be detected. We determine the root arteries heuristically by analyzing the following seven attributes of each segment:

1. **Length l_i:** The main arteries are longer than the other segments.
2. **Position on the z-axis u_i:** The main arteries supply the CoW from below. Therefore, their positions on the z-axis are likely to be lower than those of the other arteries in their subtrees.
3. **Centrality on the x-axis v_i:** This attribute is used for identifying the BA since it has a medial position on the x-axis. We thereby use the c_{BA} value from the coronal plane. The centrality is calculated from the average distance of a segment to the c_{BA} by only considering the x-components of the positions.
4. **Distance to the centroid of the subtree d_i:** The centroid is usually close to its main artery since the main artery is the largest one in the subtree.
5. **Intensity values b_i:** Due to the properties of MRAs, the main arteries have the highest intensity values. b_i is the average intensity value along the segment.
6. **Vertical alignment a_i:** The main arteries run vertically upwards until they bifurcate into the CoW. A segment is approximated by a vector between start and end point a_i is calculated from the angle between this vector and the z-axis.
7. **Affiliation to the respective subtree s_i:** This is a three-dimensional vector where each component defines the affiliation of a vessel segment to the three subtrees.

Finally, we calculate the rank of each segment in the vessel graph to be selected as one of the root segments. For each subtree, the segment with the highest associated rank is selected as the root segment by using the following rank-function:

$$C_{i,j} = sgn(s_{i,j}) \cdot (l_i \cdot L_j + u_i \cdot U_j + v_i \cdot V_j + d_i \cdot D_j + b_i \cdot B_j + a_i \cdot A_j) \quad (2)$$

$C_{i,j}$ is the rank of segment i to be selected as the root of subtree j, for $j = 1,2,3$. The variable $s_{i,j}$ is the component j of the affiliation vector s of segment i. It describes to which subtree the segment i can be assigned to. The above described attributes have different ranges. Therefore, we normalize the ranges to lie between 0 and 1 in order to equalize their influence. $sgn(\cdot)$ is the sign function. $s_{i,j}$ is only positive, if a segment is part of subtree j. This guarantees that the RICA can only be considered as a candidate for the root segment of the right anterior subtree, the LICA for the left anterior subtree and the BA for the posterior subtree. The influence of the attributes is regulated by the weights L_j, U_j, V_j, D_j, B_j, A_j. The three main arteries LICA ($j = 1$), RICA ($j = 2$), and BA ($j = 3$) differ in size, location, alignment, and shape and are therefore not determined by the same attributes. For this reason, the weights have to be adjusted accordingly. We empirically determined $L_1 = L_2 = 0.4$, $U_1 = U_2 = 0.2$, $V_1 = V_2 = 0$, $D_1 = D_2 = 0.5$, $B_1 = B_2 = 0.5$, $A_1 = A_2 = 0.2$ as weights for the LICA and RICA root segments. Hereby, the centrality attribute v_i is eliminated since the LICA and the RICA are in the lateral parts of the ROI. For the BA root segment, we use the following weights $L_3 = 0.3, U_3 = 0, V_3 = 1, D_3 = 0.3, B_3 = 0.4, A_3 = 0.8$. Hereby, u_i is eliminated since the BA is not the lowest segment in the posterior subtree. Usually, the two vertebral arteries are below the BA.

5.4. Visual Mapping

The vessel graph contains information about different properties of the CoW, which have to be communicated to the user. Figure 2f displays the labeled vessel graph together with the MIP from the transverse view. This display is disadvantageous since the content cannot be fully perceived without changing the viewing direction. In this section we propose a visual mapping to abstract the CoW in such a way that it can be easily comprehended by the radiologist. Our visualization supports the physician to observe the overall configuration of the CoW, while still retaining sufficient details for an extensive analysis. Our proposed visual abstraction displays the CoW in a similar way as before, namely in a radial graph layout. The CoW consists of subtrees that are connected with each other at the leaves. We chose a circular layout that offers an effective way of displaying the subtrees inside different sectors. Figure 2g illustrates our approach, which we refer to as Circle of Willis Radar/Radial Visualization (CoWRadar).

We convert the labeled 3D vessel graph into a 2D graph representation, i.e., segments are represented by nodes and branching points by edges. Neuro-radiologists are primarily interested in the blood supply and collateral circulations, which can be easily observed in a graph representation. Furthermore, other important attributes of the segments are visually better encoded inside a node than an edge.

The main arteries are located at the center of the radial graph, at the zeroth level. Increasing level numbers indicate the direction of the blood flow. Every level is represented by a concentric circle, starting from the center and simultaneously encoding the distance of a segment to its corresponding main supplying artery. In essence, we visually depict the subsequent three different Levels of Detail (LODs) that successively provide more information:

Figure 8: Two nodes are depicted. The visual representation gives a detailed view of the attributes inside a segment. The left node depicts the LICA and the right node depicts the ACoA of the exemplar CoW shown in Figure 2g. Attributes are displayed in diagrammatic form inside the nodes with multiple circular arcs. The inner purple arc depicts the intensity range of the segment and the outer yellow arc depicts its length. Furthermore, the dark purple inner arc depicts the minimum and the bright purple arc depicts the maximum intensity value.

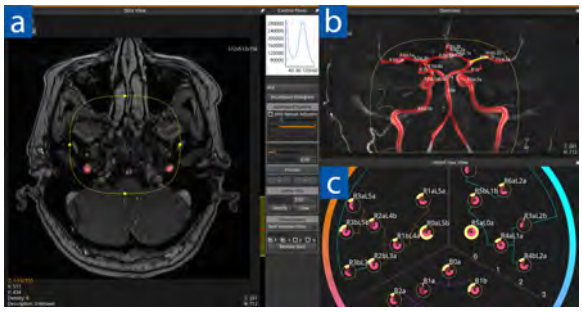

Figure 9: Screenshot of the graphical user interface developed in our work. (a) displays a multi-axial slice view. (b) displays a 3D MIP with the vessel graph overlay. (c) shows the corresponding CoWRadar.

1. **Low LOD:** The overall blood supply to an affected region of the CoW can be derived from the global arrangement of a node within a single sector. An empty sector is immediately spotted, representing a problematic blood circulation in this region. This is supposed to be a time-crucial and life-saving aspect and is, therefore, encoded at the lowest LOD to be as fast perceivable as possible (see Figure 12).
2. **Medium LOD:** At this LOD, the branching structure can be observed from the nodes and edges in the CoWRadar. The edges connecting two sectors are important since these indicate collateral blood circulation. It is a major aspect to determine if a certain region is still supplied with blood despite being not connected to its spatially closest main artery [HvdG00]. Again, this can be easily observed in our CoWRadar (see Figure 2g).
3. **High LOD:** The highest LOD offers the possibility to inspect the attributes inside the nodes, which are shown in diagrammatic form (see Figure 8). The nodes allow the radiologist to compare attributes of different segments with each other. For example, length and intensity values are displayed to provide additional information. The length allows the radiologist to distinguish between the different segments. Arteries are further differentiated by intensity values for various reasons. The main arteries are the brightest in the CoW. Low intensity values could indicate a stenosis.

The CoWRadar shown in Figure 2g can be interpreted as follows. The connection between the left anterior and right anterior sector is established by the ACoA, which we labeled as *R3aL2b*. This label consists of two labeling terms, the *R3a* term indicates that this segment is three branching points away from the RICA segment and the *L2b* term indicates that it is two branching points away from the LICA. Furthermore, each segment in the anterior subtrees is labeled from both, the RICA and LICA root segments and therefore, carries two labeling terms. The missing third label implies that the posterior subtree is not connected to the anterior subtrees. Consequently, we can assume that the PCoAs are missing on both sides.

The attributes used for the identification of the main arteries as described above can be visualized inside the nodes as circular charts, which are normalized to the respective maximum value of all segments. This layout offers a compact representation of information, while minimizing the covered space and retaining the overall topology of the CoW. Examples are given in Figure 8, showing the LICA and the ACoA. The LICA is much longer than the ACoA, which is shown by the outer yellow arc. The inner purple arc shows that the LICA has much higher intensity values than the ACoA. The inner arcs convey the minimum and the maximum intensity values of the segment. These two attributes play an essential role in selecting the root segment since they characterize the main arteries.

6. Implementation

All steps in the proposed pipeline were implemented in a software solution for the radiologists, see Figure 9. We developed the software as an extension to the AngioVis framework [The16a]. The methods have been implemented on the CPU. We use OpenGL and Qt to render the geometrical elements of the visualization. The software processes the data sets automatically and requires the radiologist only to read-in the data set and start the pipeline. The radiologist uses multiple slice views and a MIP for the traditional inspection of the data set. They are implemented in the software and linked to the CoWRadar in order to contextualize the information in the visualization. The CoWRadar provides diagnostic assistance through an additional view. In this way, it complements the workflow of the radiologist, but does not change it. Currently, a data set is processed in 55 seconds on average. The sizes of these data sets are between $448 \times 512 \times 64$ and $512 \times 512 \times 156$ voxels. The voxels are represented by *16 bit unsigned integers*. The time measurements were done on an Intel Core i5 with 3.4 GHz and 16 GB system memory.

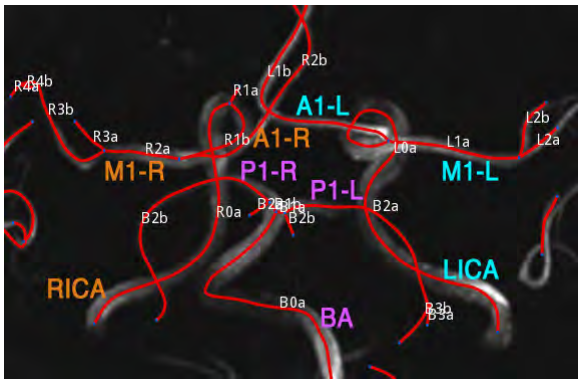

(a) Vessel graph with anatomical labels

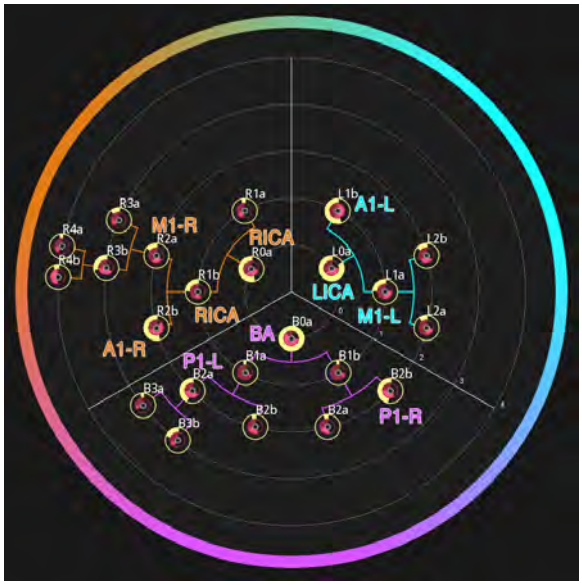

(b) CoWRadar with labels

Figure 10: An example CoW where every segment is correctly identified by our approach. We manually added the Latin names in order to show the correspondences between the original data set and our CoWRadar.

(a) Transverse MIP

(b) Subtrees

(c) CoWRadar

Figure 11: In this patient 91% of the arteries could be correctly identified using our proposed method. (a) shows a transverse MIP indicating a missing left PCoA (yellow arrow). (b) illustrates the subdivision result and (c) shows the CoWRadar with the ACoA (yellow arrow) connecting both anterior subtrees.

7. Results

The data sets were acquired from patients with various diseases such as brain tumors or other cerebrovascular diseases, with the majority being suspected stroke patients. All data sets have been automatically processed using our proposed approach, without any manual interventions or adjustments.

In the first example (see Figure 10), we present a case where all three communicating arteries are missing according to the gold standard. This circumstance is successfully depicted in our CoWRadar. As the communicating arteries are absent, there are no connections between the three sectors. We manually annotated the vessel graph and the CoWRadar with the Latin names of the segments in order to show their correspondences. In the second example (see Figure 11) 91% of the segments were correctly identified. According to the gold standard, all arteries of the CoW are present in this data set, except for the left PCoA. As depicted in the transverse MIP (see Figure 11a), the left PCoA is the only artery missing, which is indicated by the yellow arrow. The separation into the three subtrees is shown in Figure 11b and the CoWRadar is presented in Figure 11c. The arc-shaped connection between the two anterior subtrees indicates the presence of the ACoA (yellow arrow in Figure 11c). The right P1 segment could not be identified due to low intensity values. The right PCoA is correctly detected but not represented by a

(a) Transverse MIP (b) Subtrees

(c) CoWRadar

Figure 12: Limitations of our approach. In this subject only 58% of the arteries could be correctly identified with the proposed method.

connection to the posterior sector since the right P1 segment is not correctly identified.

The third example (see Figure 12) demonstrates the limitations of our proposed method. According to the gold standard, the LICA is missing as shown in Figure 4a. The only other missing artery is the ACoA. We correctly identified the missing LICA, but our approach does not detect the remaining arteries of the left subtree since the root segment is absent. This means that the left M1 and A1 segments will not be assigned to the left sector.

8. Evaluation

We conducted a study consisting of 63 TOF-MRA data sets that were investigated by an expert neuro-radiologist and three volunteering radiologists. The neuro-radiologist, being much more experienced than the three radiologists, created the gold standard. For the study, the radiologists analyzed the raw data on their workstations and marked the twelve arterial segments in a standardized questionnaire as being present or absent. We compared the findings of our approach and the findings of the radiologists to the gold standard and calculated the sensitivity, specificity and negative predictive value to evaluate the results.

The separate evaluation of the main arteries and the entire CoW is motivated by the way our approach works. We propose a method that automatically identifies the main arteries by certain attributes. The remaining arteries are not directly identified but labeled with our systematic labeling approach. Our method displays their connections to the main arteries and the branching structure that lies in-between, hence the arteries are visually described.

The sensitivity metric, or true positive rate, measures the proportion of existing segments that could be correctly identified. The specificity metric, or true negative rate, measures the proportion of missing arteries that could be detected as absent. Finally, the negative predictive value is the proportion of the correctly classified absent arteries. For a comprehensive evaluation of our approach, all three of these metrics have to be analyzed. The visualizations of the 63 data sets were presented to the neuro-radiologist for interpretation and verification if the arteries could be correctly detected by our approach.

The **sensitivity** values are shown in Figure 13a. The sensitivity value demonstrates the ability of our proposed method to detect the presence of arteries. 80.66% of all present arteries could be detected correctly, which is slightly below the performance of the radiologists. The value is mainly decreased by arteries that are represented with low contrast.

Figure 13b shows the **specificity** values. According to the gold standard, the RICA is absent in two and the LICA is absent in one data set. All three cases have been correctly classified by our proposed method. The main arteries' specificity is therefore 100%. Overall, 115 of the total 756 arterial segments (63 data sets $\times$ 12 investigated segments) were classified as missing by the gold standard. 93.04% were correctly identified as such by our approach. The specificity of the participating radiologists is in general lower compared to our method. This is because of increased false positives. The radiologists have the highest number of false positives in the communicating arteries, which means that they tend to identify the presence of a communicating artery where the gold standard states the opposite. The main reason for the slight decrease of the specificity for all arteries is caused by a false connection between the left and right anterior subtree.

Our approach seems to favor specificity over sensitivity. This means, a segment is rather detected as missing than as being present. However, these two values do not fully demonstrate how precise our approach is in detecting the missing arteries by taking the false negatives into account.

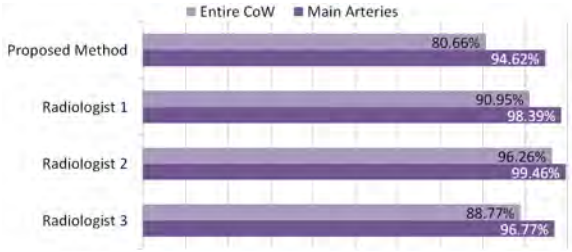

(a) Sensitivity

(b) Specificity

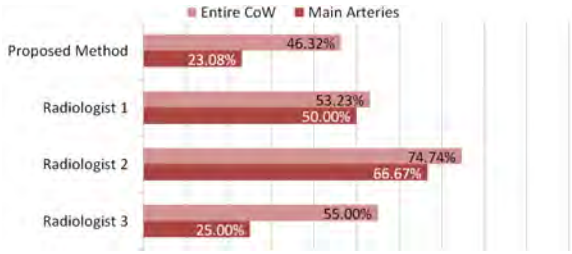

(c) Negative predictive value

Figure 13: The evaluation shows that the performance of our automatic approach is slightly below the radiologists'. (a) Sensitivity: Almost all main arteries could be correctly identified. (b) Specificity: A specificity of 93.04% for the entire CoW indicates that our approach performs better in detecting missing arteries than the radiologists. (c) The negative predictive value seems in general to be quite low.

This is given by the **negative predictive value**, which is shown in Figure 13c. The reason for the low value is the same as for the sensitivity value. Since the number of absent arteries is relatively small compared to the number of present arteries, the influence of the false negatives is much larger on the negative predictive value.

9. Limitations and Discussion

According to the evaluation our proposed method performs well in the detection of absent arteries. This is potentially of great interest for the diagnostic process since missing arteries are often the cause of problems. Our approach mostly deviates from the gold standard in those cases where the arteries are represented by relatively low intensity values. In such

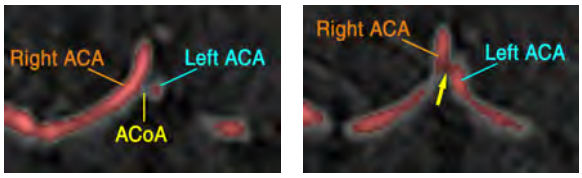

(a) Correct ACoA location. (b) Falsely detected ACoA.

Figure 14: Incorrect identification of the ACoA using our approach. (a) displays the transverse slice at z = 60 where the actual ACoA is located. Due to low intensity values, this artery could not be segmented. (b) shows the slice at z = 58, where our approach detects a false connection resulting in a connection of the two ACAs at the wrong position.

cases, the arteries are not segmented and consequently not represented in the CoWRadar. In general, the performance seems to be the lowest with the communicating arteries. The ACoA forms the connection between the two anterior subtrees, branching from the Anterior Cerebral Artery (ACA). Especially the detection of this artery poses a challenge for our approach as well as for the radiologists since it is very short and has low contrast. As Figure 14 shows, our approach is not able to correctly detect the ACoA in this patient.

The closing operation during the step 10 in the pipeline merges the two ACAs and falsely forms a connection between the left and right anterior parts, as is demonstrated in Figure 14b. Therefore, the connection is mistaken as the ACoA. In this case, the artery is considered to be falsely identified.

Another limitation of our approach is given by the way how our labeling works. If a segment is disconnected due to locally low intensity values, our approach stops the labeling at this point. This causes the remaining segments in the respective subtree to be left unlabeled or assigned to the wrong subtree.

The sample data sets are randomly selected and there was no case with an aneurysm among them. Hence, we could not test our approach on such patients. However, changes in the vasculature would probably be detected and the pathologies would be indirectly depicted by anomalies in the affected area in the CoWRadar.

One characteristic of our approach is that the outcome is controlled by multiple parameters that are heuristically motivated by the vascular anatomy. We designed these parameters together with their values based on the experience of the domain expert. We tackled the problem of over-fitting by applying our approach to unknown data sets as well. Out of the 63 data sets, only 12 are the basis for the tuning of the parameters and 51 data sets are randomly selected and were unknown before the evaluation.

10. Conclusion and Future Work

We propose an automated pipeline for the visual quantification of the CoW in stroke patients. Thereby we developed a novel method for the systematic labeling of the vessel graph. In addition, we proposed heuristics for the identification of the main arteries based on seven attributes of each segment in the vessel graph. The CoW is finally visually represented in a standardized manner in order to provide a preliminary assessment of the CoW's configuration as well as a visual indication of problematic areas. This can be used as an interface for comparisons across multiple patients.

One key aspect of our proposed workflow was to provide the CoWRadar as a standardized overview of the CoW without introducing manual processing steps for radiologists. Since the topological configuration of the CoW is the main interest during diagnosis, the CoWRadar abstracts away most of the spatial information given in the volumetric data. It only communicates the essential information to the radiologists in order to allow them a quick overview of the entire CoW in a single image. Therefore, we focused on the development of the entire pipeline, from preprocessing to visualization, instead of finding an optimal solution to a subtask in this process. For future work, it could be very interesting to see which of the steps in our pipeline could be replaced with different approaches in order to improve the final result.

So far we compared our technique against radiologists, but not how they would perform by using the CoWRadar. In the future we plan to study whether they would increase in accuracy and speed of diagnosis when accompanied by the CoWRadar. Another interesting challenge would be to process a large number of data sets with our automatic pipeline and combine the findings into a single visualization, e.g. an average CoW. This would enable the comparison of different groups of CoW.

Concluding, the evaluation demonstrated the feasibility and practicability of our approach, especially considering the heterogeneity of the data sets in the study. The domain expert stated that the findings of our proposed fully automatic method are already as good as those of a beginner radiologist.

Acknowledgments

The work presented in this paper has been supported by the Austrian Science Fund (FWF) grant no. TRP 67-N23 (Knowledge Assisted Sparse Interaction for Peripheral CT-Angiography – KASI). The data sets are courtesy of the Karl Landsteiner University of Health Sciences, Austria.

References

[BMJ*05] BULLITT E., MULLER K. E., JUNG I., LIN W., AYLWARD S.: Analyzing attributes of vessel populations. *Medical Image Analysis 9*, 1 (2005), 39–49. 2

[Bog12] BOGUNOVIC H.: *Geometric Modeling and Characterization of the Circle of Willis*. PhD thesis, Universitat Pompeu Fabra, 2012. 2

[CA05] CONDURACHE A., AACH T.: Vessel segmentation in angiograms using hysteresis thresholding. In *Proceedings of the IAPR Conference on Machine Vision Applications 2005* (2005), pp. 269–272. 2, 4

[Can86] CANNY J.: A computational approach to edge detection. *IEEE Transactions on Pattern Analysis and Machine Intelligence 8*, 6 (1986), 679–698. 2

[DLR09] DRAPER G. M., LIVNAT Y., RIESENFELD R. F.: A survey of radial methods for information visualization. *IEEE Transactions on Visualization and Computer Graphics 15*, 5 (2009), 759–776. 2

[HGF11] HARTUNG M., GRIST T., FRANCOIS C.: Magnetic resonance angiography: current status and future directions. *Journal of Cardiovascular Magnetic Resonance 13*, 1 (2011), 19. 3

[HvdG00] HARTKAMP M. J., VAN DER GROND J.: Investigation of the Circle of Willis using MR angiography. *MedicaMundi 44*, 1 (2000), 20–27. 2, 8

[KQ03] KIRBAS C., QUEK F. K. H.: Vessel extraction techniques and algorithms: A survey. In *Proceedings of the IEEE Symposium on Bioinformatics and Bioengineering* (2003), pp. 238–245. 2

[LKC94] LEE T.-C., KASHYAP R. L., CHU C.-N.: Building skeleton models via 3-D medial surface/axis thinning algorithms. *Graphical Models and Image Processing 56*, 6 (1994), 462–478. 2, 5

[Mis13] MISTELBAUER G.: *Smart Interactive Vessel Visualization in Radiology*. PhD thesis, TU Wien, 2013. 2

[MK16] MARINO J., KAUFMAN A.: Planar visualization of tree-like structures. *IEEE Transactions on Visualization and Computer Graphics 22*, 1 (2016), 906–915. 2

[MMNG15] MIAO H., MISTELBAUER G., NAŠEL C., GRÖLLER M. E.: CoWRadar: Visual quantification of the circle of willis in stroke patients. In *Proceedings of Eurographics Workshop on Visual Computing for Biology and Medicine 2015 (EG VCBM)* (2015), pp. 1–10. 2

[NGB*09] NEUGEBAUER M., GASTEIGER R., BEUING O., DIEHL V., SKALEJ M., PREIM B.: Map displays for the analysis of scalar data on cerebral aneurysm surfaces. *Computer Graphics Forum 28*, 3 (2009), 895–902. 2

[PB13] PREIM B., BOTHA C. P.: *Visual Computing for Medicine*. Elsevier, 2013. 2

[Poc04] POCK T.: *Robust Segmentation of Tubular Structures in 3D Volume Data*. Master's thesis, Graz University of Technology, 2004. 2, 5

[Tam14] TAMASSIA R.: *Handbook of Graph Drawing and Visualization*. CRC Press, 2014. 2

[TBB*07] TERMEER M., BESCÓS J. O., BREEUWER M., VILANOVA A., GERRITSEN F., GRÖLLER E.: CoViCAD: Comprehensive visualization of coronary artery disease. *IEEE Transactions on Visualization and Computer Graphics 13*, 6 (2007), 1632–1639. 2

[TC06] TANG W., CHUNG A.: Cerebral vascular tree matching of 3D-RA data based on tree edit distance. In *Medical Imaging and Augmented Reality*, vol. 4091 of *Lecture Notes in Computer Science*. Springer, 2006, pp. 116–123. 2

[The16a] THE ANGIOVIS FRAMEWORK:. http://www.angiovis.org/, June 2016. 8

[The16b] THE TOP 10 CAUSES OF DEATH, WORLD HEALTH ORGANIZATION:. http://www.who.int/mediacentre/factsheets/fs310/en/, June 2016. 1